Structural Changes Evidenced by Rheology in PP*g*MA Nanocomposites During Oxidative Ageing

F. Fordiani,[1] T. Aubry,[2] Y. Grohens[1]

[1]*Laboratoire d'Ingenierie des Materiaux de Bretagne LIMATB, Université de Bretagne SUD, UEB, Rue de Saint-Maudé, 56 325 Lorient, France*
[2]*Laboratoire d'Ingenierie des Materiaux de Bretagne LIMATB, Université de Bretagne-Occidentale, UEB, 6, avenue Victor Le Gorgeu, CS 9383, 29238 Brest Cedex 3, France*

Received 28 March 2009; accepted 23 June 2009
DOI 10.1002/app.30999
Published online 19 August 2009 in Wiley InterScience (www.interscience.wiley.com).

ABSTRACT: Maleic anhydride grafted polypropylene (PP*g*MA) reinforced by layered silicates was studied using rheological investigation techniques, to probe the degree of exfoliation of the clay particles in the melt state at 190°C. The rheological properties of the composites were investigated as a function of the ageing time and interpreted in terms of degree of dispersion of the clay platelets in the maleic anhydride modified polypropylene matrix. The interpretation in terms of exfoliation degree was confirmed by wide angle X-ray scattering and nano-secondary ions mass spectroscopy experiments. Chemical reaction, promoted by oxygen, of maleic anhydride with hydroxyl groups located on clay platelet edges, is one of the major mechanisms involved in the exfoliation process highlighted in this study. PP chain segment thermal motions as well as moderate shear were shown to be required in order to achieve clay exfoliation. © 2009 Wiley Periodicals, Inc. J Appl Polym Sci 114: 4011–4019, 2009

Key words: nanocomposites; rheology; grafting; annealing

INTRODUCTION

In recent years, polymer-layered silicate (PLS) nanocomposites, especially those containing organo-modified clays have attracted a great academic and industrial interest. They often exhibit outstanding properties such as reduced gas permeability, improved solvent resistance, superior mechanical properties, and enhanced flame retardant properties.[1]

Two major findings have aroused particular industrial interest for these materials: the first one is the successful elaboration of a real nylon-6/montmorillonite (MMT) nanocomposite by the Toyota research group in the 90s[2] and the second one is the possibility to prepare PLS nanocomposites via melt mixing without using any organic solvent, as shown by Vaia et al.[3]

Polypropylene (PP) is one of the most widely used polymers because of its large availability, relative low cost, and easy processability. Unfortunately, the apolarity and the low surface tension of PP is a major drawback regarding the dispersion of hydrophilic clay. To improve the compatibility between clay and PP chains during melt blending, polar groups such as maleic anhydride can been grafted onto PP.[4]

The most widely used nanoclay is derived from Na^+-MMT. Cation exchange reactions with alkylammonium surfactants are classically used to give the clay an organophilic character, thus promoting compatibility between hydrophobic polymers and MMT.

Different factors can affect the final structure of PLS nanocomposites: the nature of the organo-modified layered silicate (OLS), the compatibilizer, and the polymer matrix used,[4] the processing conditions such as speed rate, temperature, and rest time.[5] The structure may be characterized by a dispersion of numerous stacked clay platelets forming microaggregates within the polymer matrix, like in conventional microcomposites. Another type of structure, the so called intercalated one, is characterized by polymer chains inserted between clay layers so that the interlayer spacing increases without destroying the crystallographic order. In the exfoliated structure, clay layers are completely separated from each other and the individual platelets are dispersed throughout the organic matrix. In most PLS nanocomposites, a combination of these different types of structures is observed, leading to the so called partially exfoliated or partially intercalated structures.

Dramatic changes in physical and chemical properties have been shown to occur during PLS nanocomposite elaboration, as reported by Alexandre and Dubois.[6] For example, Gilman et al.[7] have

Correspondence to: Y. Grohens (yves.grohens@univ-ubs.fr).

shown the role played by the dispersion of OLS in the flammability behavior of PLS nanocomposites. Indeed an important decrease of the rate of heat release upon cone calorimeter combustion of PLS nanocomposites was attributed to the formation of a char barrier on the surface of the burning polymer. Migration of the clay platelets seems to play a key role in the improvement of flame retardancy properties.[8] The origin of this migration is assumed to be related to the strong increase of the temperature.

A crossed characterization can be very useful to follow structural modifications,[9] and rheometry was shown to be a particularly suitable tool to assess the state of dispersion of nanocomposites in the melt state.[10] Galgali et al.[11] have shown that creep experiments could be used to understand the microstructural changes occurring in maleic anhydride modified polypropylene (PP*g*MA)/clay nanocomposites during annealing. They have shown a gradual decrease in time of creep compliance for nanocomposites with PP*g*MA matrix and 6 wt % organo-modified clay, indicative of subtle microstructural changes occurring under almost zero-shear conditions. Solomon et al.[12] have shown that the rheological behavior of different PP*g*MA/clay nanocomposites was very sensitive to surfactant chemistry, particularly when compared with the small effects obtained using wide angle X-ray scattering. Authors have shown that the transient reversal stress response in flow reversal experiments exhibited a stress overshoot whose magnitude increased with annealing time. Furthermore, transient stresses were shown to depend on clay loading and applied strain. Rohlmann et al.[13] showed that the annealing process did not induce microstructural changes for nanocomposites containing <5% of clay, with PP*g*MA to clay ratio 1 : 1. Other authors[11–14] have calculated the flow activation energy of polymer matrix and corresponding nanocomposites and attributed the solid-like behavior of the annealed PP*g*MA/clay nanocomposites to the strong frictional interactions between OLS particles above the percolation threshold, rather than to confinement effects. In the aforementioned articles, no evidence of the influence of the atmosphere was reported.

However, Camino and coworkers,[15] using *in situ* high-temperature X-ray diffraction have shown that heating induced structural changes in EVA/clay nanocomposites, which were strongly influenced by the atmosphere during the thermal treatment. The authors have shown that nitrogen atmosphere yields no structural modification, whereas under oxygen the nanocomposite structure evolved. Using infrared spectroscopy, Zammarano et al.[16] have observed a significant migration of clay particles in PP*g*MA/clay nanocomposites, during annealing under oxidative atmosphere at a temperature above the melting point. Tidjani et al.[17] have carried out melt blending of PP*g*MA/nanocomposites under both nitrogen and air. They showed that, for samples prepared under air, X-ray peaks disappeared, suggesting significant delamination of clay particles, whereas samples produced under nitrogen exhibited a rather intercalated structure.

All these articles only provided a partial scattered view of the thermally stimulated structural changes in PP*g*MA/clay systems. Using infrared spectroscopy, melt rheology, and nano-secondary ions mass spectroscopy (nano-SIMS), a multiscale approach was undertaken in our study. Our aim is to evidence the chemical and physical mechanisms that yield the platelets migration and structural changes in PP*g*MA/clay nanocomposites, which occur during thermal treatment.

EXPERIMENTS

Materials

PP, grade EXXTRAL BNT013 supplied by ExxonMobil (Courbevoie, France) was used in this study. Number-average molecular weight (M_n) is 245×10^3 g mol^{-1} and the polydispersity index is 2.9. The melting point of the PP is 160°C. PP*g*MA containing 1 wt % of maleic anhydride, referenced as Orevac CA100 and supplied by Arkema (Serquigny, France), was used as a compatibilizer. The number-average molecular weight of Orevac is 8.2×10^3 g mol^{-1} and the polydispersity index is 10.

Cloisite C15A modified clay was already used in previous works with PP.[18] Cloisite C15A is a natural MMT modified with a dimethyl, benzyl, hydrogenated tallow, and quaternary ammonium salt. The clay is supplied by Southern Clay Products (Gonzales, TX). A thermogravimetric analysis performed on the clay shows that it contains 38 wt % of organic material. All materials were dried under vacuum overnight at 80°C before use.

Nanocomposite preparation

PP and PP*g*MA have been used by Lertwimolnun and Vergnes[19] in their work on PP-based nanocomposites. According to the authors, the clay aggregates become smaller and silicate layers are finely dispersed for concentrations of PP*g*MA between 10 and 25 wt %. As grafted PP has shorter molecular weight and higher polydispersity than PP, blends with low PP*g*MA content are generally used.[19] Thus, a PP/PP*g*MA mass ratio 80/20 was chosen in this work. The polymer samples were melt-extruded using a Brabender twin-screw compounder DSK 42/6 with three different zones operated at 180, 180, and 190°C, respectively, (from hopper to die) and a

screw speed of 60 rpm. The preparation of polymer nanocomposites, containing 3 wt % Cloisite 15A, was performed using melt blending, under the same processing conditions as those reported earlier for the PP/PP*g*MA blends. To improve the clay dispersion, PP*g*MA/clay nanocomposites studied in this work have been extruded twice. The collected samples were pelletized and then test specimens were prepared by compression molding at 190°C during 5 min. The thickness of the films is 100 ± 20 microns.

Instrumentation

Wide angle X-ray diffraction

The X-ray diffraction analysis was performed at ambient temperature using a X'Pert PRO PANalytical, with nickel-filtered Cu Kα radiation of wavelength 1.54 Å, operated at 35 KV and 20 mA. The diffraction intensity data were collected automatically using a 2θ mode with a step-scanning method (step-width of 1.07° and 4 s intervals) in the diffraction range 3–70°.

Nano-secondary ion mass spectrometry

The analysis was carried out using a Cameca nano-SIMS 50 equipped with a microbeam cesium ion source working at 16 keV Cs^+ and high-mass resolution. The probe lateral resolution for the $^{133}Cs^+$ ion source used is about 50 nm. We carried out a 2D "image" (map) of the surface distribution of secondary ion species to determine the concentration and to localize the distribution of clay and intercalant molecules within the polymer matrix. The signature of the clay and intercalant are the isotope ^{28}Si and the isotopes $^{12}C/^{14}N$, respectively.

Polymer-nanocomposite samples were covered by a gold thin layer before analysis.

Melt rheology

A Bohlin CVO rheometer equipped with an extended temperature cell and a 25 mm diameter parallel plate geometry was used. The gap was fixed at 1 mm and the experiments were performed at a fixed temperature of 190°C. For neat PP*g*MA and PP-based nanocomposites, the limit of the linear viscoelastic regime was determined by performing a strain sweep at 1 Hz. Linear viscoelastic measurements were performed over a frequency range of 0.01–10 Hz. Time sweep tests at a frequency of 1 Hz were also carried out. A strain of 1% was shown to lie in the linear viscoelastic domain for all samples, and was applied for all viscoelastic measurements carried out in this study. The thermal history was erased by equilibrating all samples at 190°C for 5 min.

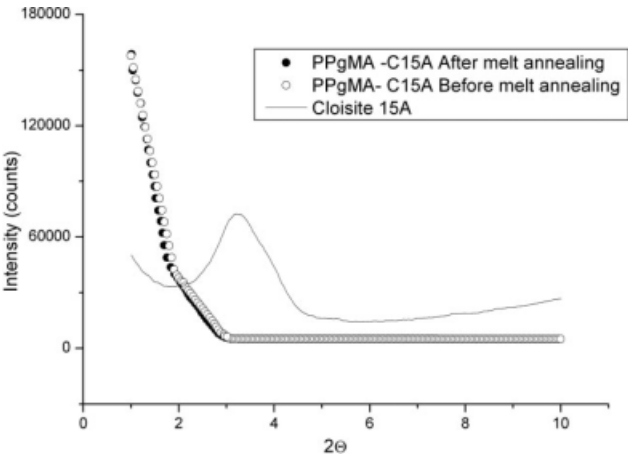

Figure 1 Comparison between XRD patterns of PP*g*MA-C15A nanocomposites before and after melt annealing.

Thermal analysis

Thermogravimetric analysis was performed using a ATG SETARAM TG-DTA 92-10 with a heating ramp of 20°/min under nitrogen flow, from room temperature up to 800°C.

Infrared spectroscopy

Fourier transform infrared spectroscopy (FTIR) was performed using a PerkinElmer (Spectrum 1000) spectrophotometer in transmission mode. Spectra were signal averaged over 128 scans at a resolution of 4 cm^{-1}. Before and after annealing, samples were hot pressed to obtain 50-μm thin films.

RESULTS AND DISCUSSION

XRD analysis

XRD analyses are plotted in Figure 1. The angular dependence of the diffracting intensity is reported for PP*g*MA/C15A before and after thermal treatment under oxidative atmosphere. The peak corresponding to {001} basal reflection of C15A is situated at $2\theta = 3.41$ ($d_{001} = 25.8$ Å). Results show that directly after extrusion ("PP*g*MA/C15 before melt annealing" sample) X-ray {001} peaks disappear, indicating that at least partial delamination of the layered structure is obtained. No modification of the X-ray spectra is observed on the PP*g*MA/C15 after melt annealing. This result is consistent with results reported by Tidjani et al.[17] on PP*g*MA/nanomer I28E nanocomposites obtained by melt blending under air.

Further information on the possible thermal treatment effects on PP*g*MA/C15A nanocomposite structures are expected from rheology. Indeed, rheology in the melt state, as previously observed by Solomon et al.[12]working on different OLS/PP*g*MA samples, is

very sensitive to the structure, particle shape, and surface characteristics of the dispersed phase.

Rheological characterization

Evidence of degradation

During thermal treatment, like annealing at temperatures above the melting point, several phenomena take place that can affect the final morphology of the PLS nanocomposites. Thermal degradation of the surfactant, used to intercalate the pristine clay, and polymer oxidation can induce structural changes in the polymer matrix. As shown by several authors, these phenomena can be strongly influenced by the atmosphere.[15,16]

To study the degradation kinetics,[20] we performed time sweep tests during annealing at 190°C (Fig. 2). Both elastic and loss moduli dramatically increased under oxidative atmosphere, whereas under nitrogen environment, elastic and loss moduli reached quasi steady-state values within a few minutes. Under oxidative conditions, chemical reactions between the OLS and the polymer matrix and/or microstructural rearrangements of OLS can yield the increase of the G' and G'' observed in Figure 2. To further understand this behavior, we performed a series of dynamic sweep test.

Effect of nanoparticles on degradation

Comparison between the linear viscoelastic response of PP*g*MA and that of PP*g*MA/C15A nanocomposite shows the significant effect of adding nanoclay particles. Frequency dependence of elastic and loss moduli of the two systems is compared in Figure 3. Over the whole frequency range investigated, and especially at low frequencies, PP*g*MA/nanocomposites have higher elastic and loss moduli compared with pure PP*g*MA. Moreover, a tendency to plateau can be observed at low frequencies for PP*g*MA/C15A nanocomposite. This pseudo solid-like behavior could be attributed to the existence of a percolation network.[11] The effect of the annealing process on the PP*g*MA/C15A nanocomposites, under oxidative atmosphere, was then investigated. In Figure 4, we reported G' versus frequency curve evolution during a series of experiments performed on the same sample, during a total annealing time of 2 h25′ at 190°C. The annealing process clearly influenced the elastic behavior and the effect was even more pronounced at low frequencies; the tendency to low-frequency G' plateau is all the more marked as the annealing time is higher, indicative of network reinforcement during annealing. This effect looks like that obtained when increasing particle concentration of PLS nanocomposites.[12]

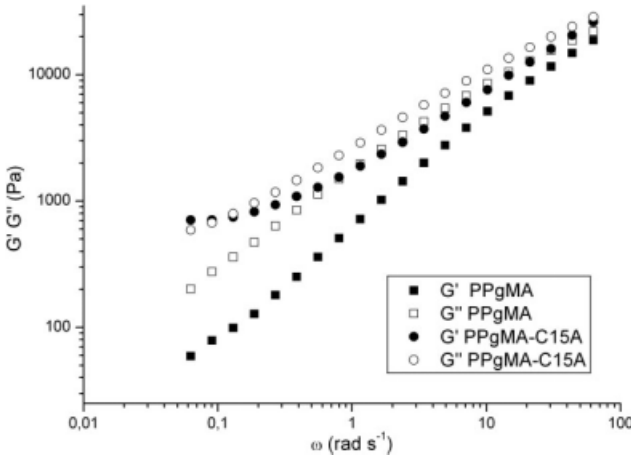

Figure 3 Elastic and loss modulus as a function of frequency for neat PP*g*MA and corresponding nanocomposites.

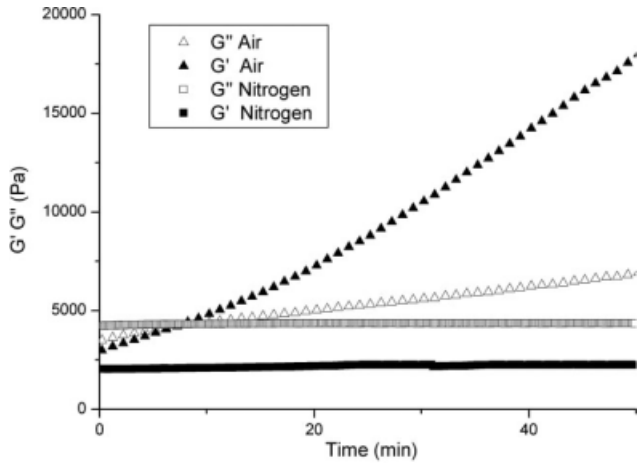

Figure 2 Elastic and loss moduli as a function of time for PP*g*MA/C15A nanocomposites under oxidative and nitrogen atmosphere.

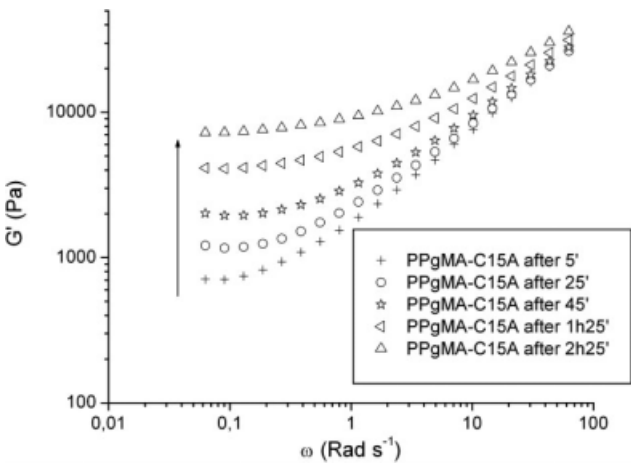

Figure 4 Elastic modulus as a function of frequency for the PP*g*MA/C15A nanocomposite during annealing at 190°C under oxidative conditions.

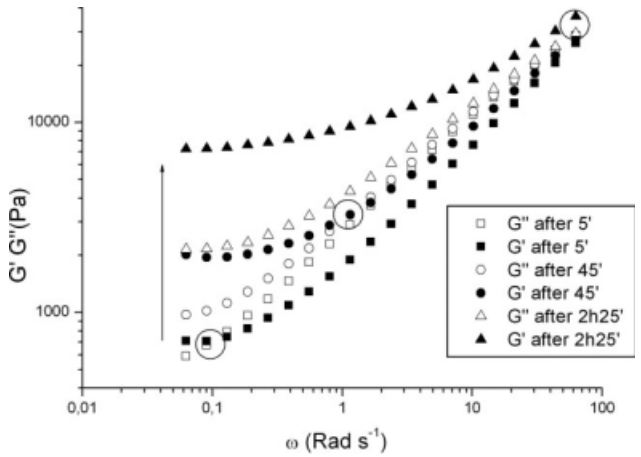

Figure 5 Elastic and loss modulus as a function of frequency for the PP*g*MA/C15A nanocomposite during annealing at 190°C under oxidative conditions: determination of G' and G'' crossover.

In Figure 5, the linear viscoelastic moduli of PP*g*MA/clay nanocomposites were reported as a function of frequency, for three different annealing times, to determine the G', G'' crossover, marking the transition from a liquid-like ($G' < G''$) to a solid-like ($G' > G''$) behavior. As shown in Figure 5, the crossover frequency of PP*g*MA/C15A nanocomposites shifts toward higher frequencies with increasing annealing time, which tends to show that thermal treatment increases the connectivity, and therefore the elasticity, of the particle network.

Under nitrogen, Galgali et al.[11] observed an increase of the G' low-frequency plateau, during annealing, for clay content above 9%. Surprisingly, during annealing, they observed a significant decrease of G' for a clay content of 3%. Also, Rohlmann et al.[13] observed no effects of the presence of the OLS during annealing, for clay contents up to 5% and concluded that a minimum amount of exfoliated platelets was needed to get such effects. If we compare these rheological results, obtained under a nitrogen atmosphere, with our results under air, we can conclude that an oxidative atmosphere can significantly perturb the structure within PLS nanocomposites, even at low-clay fractions. Similar conclusions have been drawn by Lewin et al., using XRD investigation technique. Indeed, they observed an increase of the clay interlayer spacing during annealing, and argued that, under oxidative conditions, partial oxidation of the polymer yields an increase in polarity of the matrix, promoting the intercalation of PP chains into the clay gallery.

Vaia and coworkers[21] have shown, using TGA-MS, that the degradation temperature of alkyl quaternary ammonium MMT is around 180°C. They claimed that the stability of the C—N linkage could be affected by different factors such as temperature, presence of catalytic species, and coreactants like oxygen. Dharaya and Jana[22] have shown, by contact angle measurement, a decrease in polarity of alkyl quaternary ammonium MMT during annealing at 250°C, and proved that polarity of the clay decreased with thermal decomposition of the intercalant. Therefore, it can be argued that, under oxidative conditions, the increase in polarity of the PP matrix, combined with the decrease of the OLS polarity, leads to a better affinity between polymer and organo-modified clay.

Physico–chemical and mechanical effects on degradation

To discriminate different possible effects responsible for microstructural evolution induced by annealing under oxidative atmosphere, effects of polymer matrix degradation, intercalant decomposition, and shear, on the linear viscoelastic behavior of the nanocomposites were studied.

It is well known that grafting maleic anhydride onto PP matrix leads to chain scission and consequently to a decrease of molar mass, leading to a decrease of viscosity.[11–13] In the systems we studied, PP*g*MA degradation should thus lead to a lowering in the complex viscosity. Having shown that the annealing process had no effects on the linear viscoelastic response of PP*g*MA, we then exclude any influence of the polymer matrix degradation on the microstructural changes in the nanocomposites.

The thermal degradation of the intercalant might also play an important role on the structural changes during annealing process. To check this hypothesis, we have calcinated Cloisite C15A at 600°C for 1 h to remove most of the organic alkyl ammonium surfactant. The PLS nanocomposites were then prepared with the calcinated clay, following the procedure previously described, and a frequency sweep oscillatory shear test was performed after annealing. Figure 6 shows the influence of the calcination process on the linear viscoelastic response of the PP*g*MA/clay nanocomposite; only the tests before annealing and after 1 h annealing were reported. No significant evolution of G' and G'', before and after thermal treatment, is evidenced, over the whole range of frequency investigated. This result shows that the intercalated alkyl ammonium ions play a role on mechanism governing the structural changes during annealing. However, calcination of Cloisite is known to modify the surface chemistry and structure of the clay and calcinated Cloisite certainly does not behave as standard Cloisite in the PP*g*MA matrix; so that the only conclusion that can be drawn from this experiment is that organic intercalant is required to ensure the platelet dispersion during the annealing process under air atmosphere.

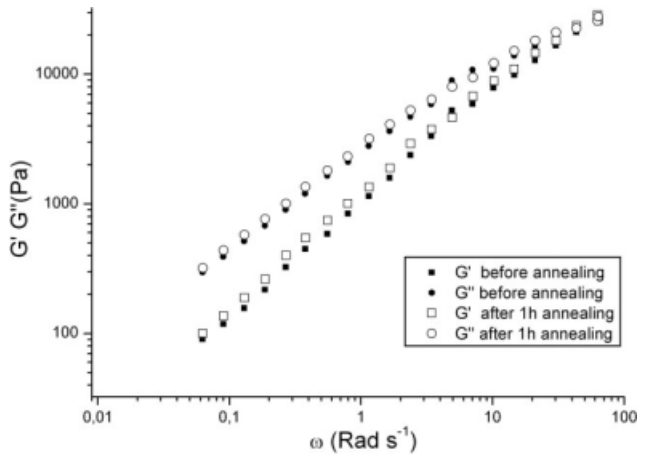

Figure 6 Influence of calcination process on the linear viscoelastic response of the PP*g*MA/clay nanocomposite.

Shear is also known to have an influence, as demonstrated by Zhang et al.[23] on the dispersion of OLS in a PP*g*MA matrix: shear can indeed induce an increase of exfoliation degree. Figure 7 shows the elastic modulus G' as a function of frequency for PP*g*MA/C15A nanocomposites for the same annealing times at 190°C, with or without applied shear. This figure shows that shear has an influence on the thermal degradation of the nanocomposites during annealing: the G' low-frequency plateau level slightly increases under shear. However, the most significant factor seems to be the annealing time.

Figure 8 shows the complex viscosity as a function of frequency for the PP*g*MA/clay nanocomposite during annealing at 190°C under oxidative conditions. The dynamic flow curve exhibits an apparent yield stress for the PP*g*MA/C15A nanocomposites. To fit this behavior, a Carreau–Yasuda model with a yield stress was used, as suggested by Berzin et al.[24] and Lertwimolnun and Vergnes[25]:

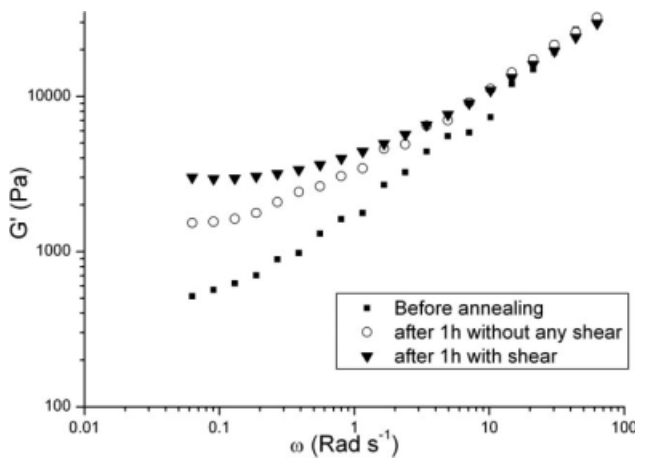

Figure 7 Elastic modulus G' as a function of frequency for PP*g*MA/C15A nanocomposites for 1 h annealing times at 190°C, with and without applied shear.

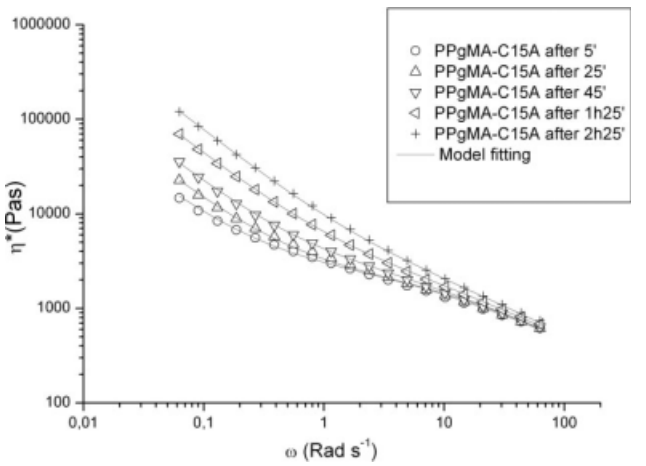

Figure 8 Complex viscosity as a function of frequency for the PP*g*MA/C15A nanocomposite during annealing at 190°C under oxidative conditions.

$$\eta^*(\omega) = \frac{\sigma_0}{\omega} + \eta_0[1 + (\lambda\omega)^a]^{\left(\frac{n-1}{a}\right)} \quad (1)$$

where σ_0 is the yield stress, η_0 is the zero-shear viscosity, λ is a time constant, the power-law exponent is $(n - 1)$ and the Yasuda parameter a is related to the width of the transition region between the Newtonian region characterized by η_0 and the power-law region. To obtain the best fit, the five adjustable parameters were determined using the linear statistical model based on total sum of squares.

Figure 8 shows the perfect agreement between the experimental data of $\eta^*(\omega)$ and the Carreau–Yasuda model. The parameters of the Carreau–Yasuda model with yield stress are reported in Table I. The apparent yield stress is shown to control the rheological response and clearly appears as a relevant material parameter. It has been plotted as a function of annealing time in Figure 9: the dependence is nearly linear. The apparent yield stress σ_0 has been shown to be related to the degree of exfoliation for PLS/nanocomposites,[25] and therefore, Figure 9

TABLE I
Parameters of the Carreau–Yasuda Model with Yield Stress Used to Fit the Experimental Data of PP*g*MA/C15A Nanocomposites During Annealing

Melt annealing time	η_0 (Pa s)	λ	A	n	σ_0 (Pa)
5′	2700	0.2	0.8	0.43	800
25′	2300	0.1	0.8	0.35	1280
45′	2300	0.1	0.8	0.35	2000
1 h05′	2300	0.1	0.8	0.35	3000
1 h25′	2300	0.1	0.8	0.35	4200
1 h45′	2300	0.1	0.8	0.35	5300
2 h05′	2300	0.1	0.8	0.35	6400
2 h25′	2300	0.1	0.8	0.35	7500

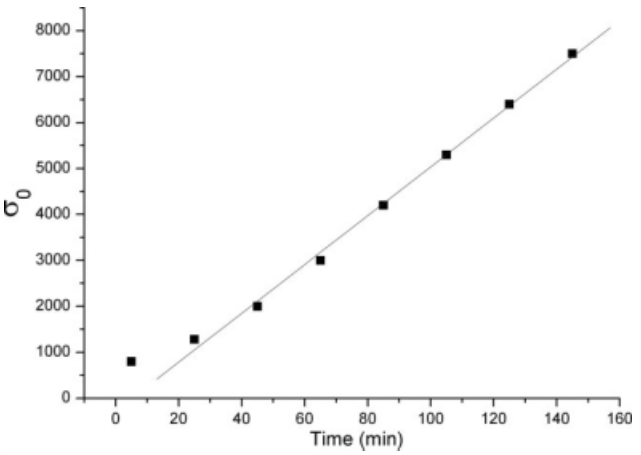

Figure 9 Apparent yield stress as a function of annealing time for PP*g*MA/C15A nanocomposite.

confirms that the microstructure of the PP*g*MA/C15A nanocomposites is significantly dependent on annealing time.

Infrared spectroscopy

Microstructural evolutions, suggested by the rheological study of annealed nanocomposite samples, are most likely due to chemical reactions between the polymer matrix and the OLS. To investigate the chemical changes during annealing, FTIR spectroscopy was carried out. The general evolution of the IR spectra of PP*g*MA nanocomposites films, before and after annealing in the presence of oxygen, is presented in Figure 10. Because of the difficulty of obtaining films with exactly the same thickness, spectra were normalized using an internal standard peak at 1304 cm^{-1}, making the analysis only qualitative. Before annealing, the sample FTIR spectrum presents a shoulder on the carbonyl band at 1780 cm^{-1} that can be assigned to the carbonyl group of the maleic anhydride ring, tending to prove that the thermal treatment produces a ring opening. Moreover, the spectrum is mainly characterized by an increase of absorbance in the carbonyl regions with a maximum at 1720 cm^{-1} and two shoulders at 1715 and 1735 cm^{-1}. The main absorption at 1720 cm^{-1} might be attributed to the formation of ketone groups and the first shoulder at 1715 cm^{-1} to a partial hydrolysis of the anhydride functions that produces carboxylic acids in the dimer form. The second shoulder at 1735 cm^{-1} might be attributed to the ester or to the carbonyl vibration of carboxylic acids associated with hydroxyl groups.[26] These results clearly indicate that maleic anhydride have not completely reacted during the melt extrusion process. During annealing, maleic anhydride ring opening and the reaction of carboxylic acids with hydroxyl groups present on the edge of the clay occurs as depicted in Figure 11. This chemical reaction yields grafting of the PP*g*MA chains on clay platelets, which leads to a peeling off effect, and therefore to a better dispersion of the OLS as presented in Figure 12.

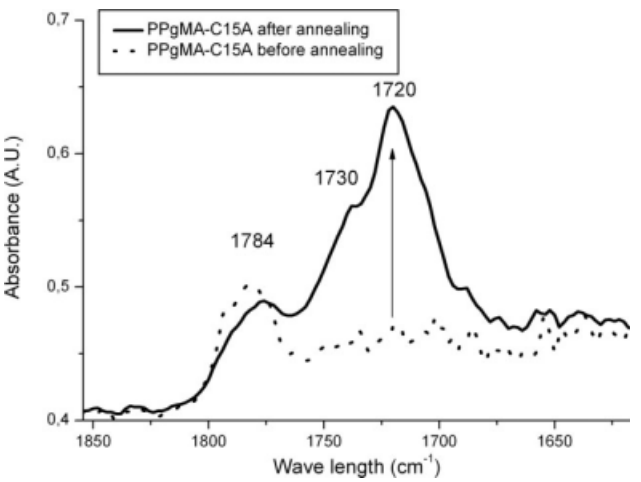

Figure 10 FTIR spectrum of PP*g*MA/C15A nanocomposite films before and after annealing under oxidative conditions.

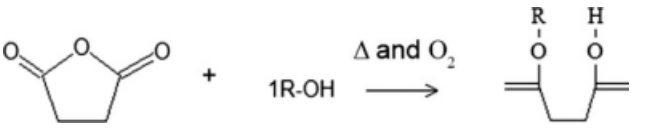

Figure 11 Schematic reaction between carboxylic acids of maleic anhydride and hydroxyl groups present at the edge of clay platelets.

Nano-SIMS

A comparative study of the structure of PP*g*MA/C15A nanocomposites, before and after annealing, was performed using nano-SIMS. This technique, allowing ion imaging of microtomed samples, is classically used for the study of trace elements in biological tissues[27]; in this work, it was used to determine the concentration and to localize the

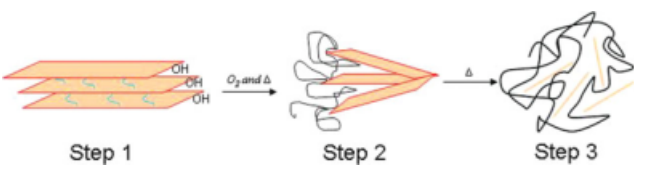

Figure 12 Schematic description of the exfoliation process: Step 1, hydroxyl groups at the edges of the platelets; Step 2, grafting and peeling; Step 3, dispersion of clay platelets in the PP melt. [Color figure can be viewed in the online issue, which is available at www.interscience.wiley.com.]

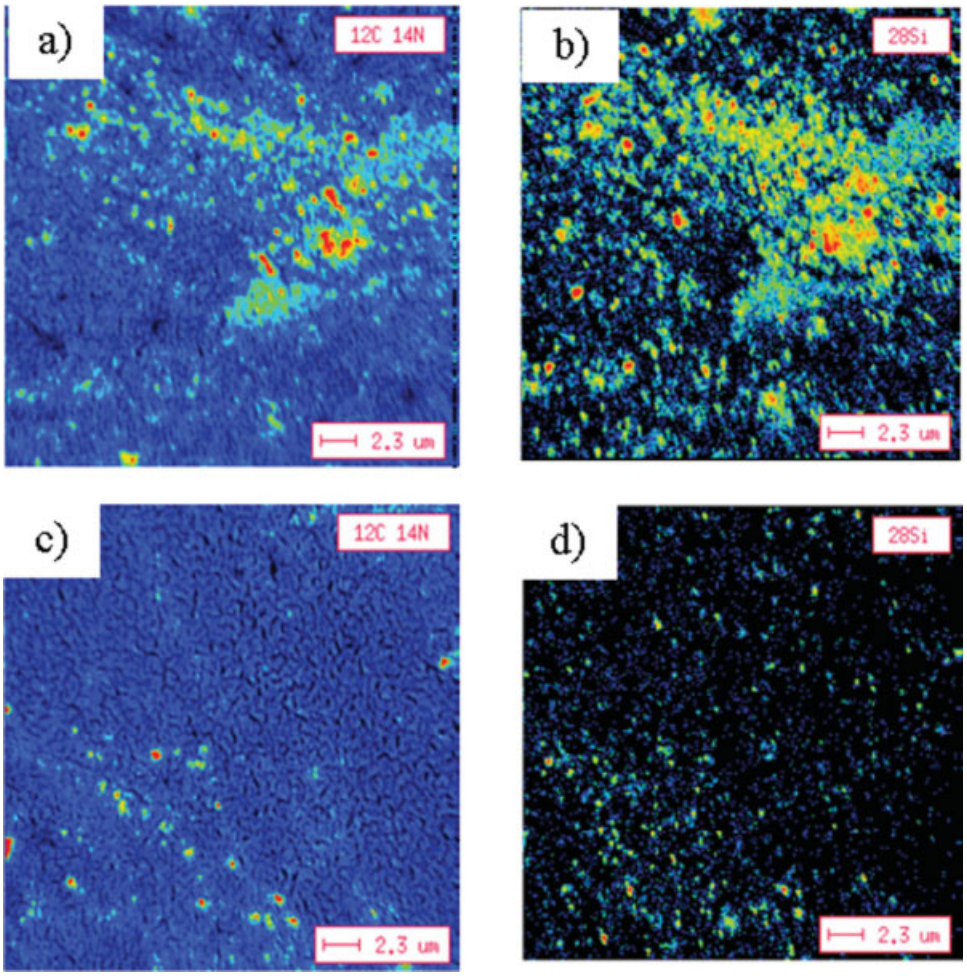

Figure 13 Nano-SIMS images of PP*g*MA/C15A nanocomposite before (a, b) and after thermal annealing (c, d). [Color figure can be viewed in the online issue, which is available at www.interscience.wiley.com.]

distribution of clay and intercalant molecules within the polymer matrix. We focused our research on ^{12}C and ^{14}N isotopes, and ^{28}Si isotope, which are the signatures of the intercalant and the clay, respectively.

Figure 13(a,b) show the isotope concentration for PP*g*MA/C15A nanocomposite films before annealing, whereas Figure 13(c,d) show the isotope concentration after annealing. Large micron scale domains with higher concentrations of aggregated clay can be clearly distinguished in the sample before annealing. Clay dispersion seems to be improved after annealing, underlying the effects of the thermal process on the microstructure of PP*g*MA/C15A nanocomposites, under oxidative atmosphere. This result is a clear signature of the platelet migration after annealing, which yields a higher level of dispersion of most platelets in the PP*g*MA matrix. Only small aggregates of platelets remain as observed in Figure 13(c,d), which indicates that exfoliation is never completely achieved even in well-designed and processed nanocomposite systems.

CONCLUSION

The interpretation of the results presented in this study is based on the peeling off mechanisms of clay stacks, promoted by oxidative ageing in the melt. Maleic anhydride groups are catalyzed in their chemical reaction with the OH groups located on the edges of the clay platelets, by oxygen/temperature/time coupling mechanisms, as revealed by FTIR experiments. As valence bonds are created between platelets and PP*g*MA chain segments, their thermal mobility acts as a driving force to separate the clay stacks, leading to a significant reinforcement of the percolation network elasticity, as probed by rheology. Moreover, the enhanced mobility of the grafted clay platelets acts also on a large length scale, because the micron scale dispersion was shown to be affected. Indeed, nano-SIMS provided evidence that Cloisite 15 A aggregates were better dispersed in the PP*g*MA matrix after thermal oxidative treatment.

The authors thank Professor Brendlé for wide angle X-ray diffraction measurement. They also thank Thomas Delhaye for the nano-SIMS analysis and Europe for funding.

References

1. Sinha, R.; Okamoto, M. Prog Polym Sci 2003, 28, 1539.
2. Okada, A.; Usuki, A.; Kojima, Y.; Kurauchi, T.; Kamigaito, O. MRS Symp Proc 1990, 171, 45.
3. Vaia, R. A.; Ishii, H.; Giannelis, E. P. Chem Mater 1993, 5, 1694.
4. Kawasumi, M.; Hasegawa, N.; Kato, M.; Usuki, A.; Okada, A. Macromolecules 1997, 30, 6333.
5. Lertwimolnun, W.; Vergnes, B. Polym Eng Sci 2007, 47, 2100.
6. Alexandre, M.; Dubois, P. Mater Sci Eng 2000, 28, 1.
7. Gilman, J.; Kashiwagi, T.; Morgan, A. B.; Harris, R. H.; Brassell, L.; Awad, W. H.; Davis, R. D.; Chyall, L.; Sutto, T.; Trulove, P. C.; Delong, H. Fire Mater 2001, 28, 273.
8. Tang, Y.; Lewin, M. Polym Degrad Stab 2007, 92, 53.
9. Samyn, F.; Bourbigot, S.; Jama, C.; Bellayer, S.; Nazare, S.; Hull, R.; Castrovinci, A.; Fina, A.; Camino, G. Eur Polym J 2008, 44, 1642.
10. Krishnamoorti, R.; Yurekli, K. Curr Opin Colloid Interface Sci 2001, 6, 464.
11. Galgali, G.; Ramesh, C.; Lele, A. Macromolecules 2001, 34, 852.
12. Solomon M. J.; Almusallama, S.; Seefeldt, K. F.; Somwangthanaroj, A.; Varadan, P. Macromolecules 2001, 6, 1864.
13. Rohlmann, C. O.; Failla, M. D.; Quinzani, L. M. Polymer 2006, 47, 7795.
14. Ren, J.; Silva, A.; Krishnamoorti, R. Macromolecules 2000, 33, 3739.
15. Pastore, H. O.; Frache, A.; Boccaleri, E.; Marchese, L.; Camino, G. Macromol Mater Eng 2004, 289, 783.
16. Zammarano, M.; Giman, J. W.; Neyden, M.; Pearce, E. M.; Lewin, M. Macromol Rapid Commun 2006, 27, 693.
17. Tidjani, A.; Wald, O.; Phl, M.-M.; Hentschel, P.; Shartel, B. Polym Degrad Stab 2003, 82, 133.
18. Ton-That, M.-T.; Perrin-Sarazin, F.; Cole, K. C.; Bureau, M. N.; Denault, J. Polym Eng Sci 2004, 44, 1212.
19. Lertwimolnun, W.; Vergnes, B. Polym Eng Sci 2006, 46, 314.
20. Lim, Y. T.; Park, O. O. Macromol Rapid Commun 2000, 21, 231.
21. Xie, W.; Gao, Z.; Pan, W.-P.; Hunter, D.; Singh, A.; Vaia, R. Chem Mater 2001, 13, 2979.
22. Dharaya, D.; Jana, S. Polymer 2005, 46, 10139.
23. Zhang, Q.; Wang, Y.; Fu, Q. J Polym Sci Part B 2003, 41, 1.
24. Berzin, F.; Vergnes, B.; Delamare, L. J Appl Polym Sci 2001, 80, 1243.
25. Lertwimolnun, W.; Vergnes, B. Polymer 2005, 46, 3462.
26. Phillipart, J.-L.; Sinturel, C.; Arnaud, R.; Gardette, J.-L. Polym Degrad Stab 1999, 64, 213.
27. Audinota, J.-N.; Schneiderb, S.; Yeglesb, M.; Hallegotc, P.; Wennigb, R.; Migeon, H.-N. Appl Surf Sci 2004, 231, 490.